Title

Non-Invasive Differentiation of Benign Renal Tumors from Clear Cell Renal Cell Carcinomas Using Clinically Translatable Hyperpolarized 13C Pyruvate Magnetic Resonance

Journal

Tomography, 2(1)

ISSN

2379-1381

Authors

Sriram, Renuka
Van Criekinge, Mark
DeLos Santos, Justin
et al.

Publication Date

2016-03-01

DOI

10.18383/j.tom.2016.00106

Peer reviewed

HHS Public Access

Author manuscript

Tomography. Author manuscript; available in PMC 2016 May 23.

Published in final edited form as:

Tomography. 2016 March ; 2(1): 35–42. doi:10.18383/j.tom.2016.00106.

Non-invasive differentiation of benign renal tumors from clear cell renal cell carcinomas using clinically translatable hyperpolarized ^{13}C pyruvate magnetic resonance

Renuka Sriram[1], **Mark Van Criekinge**[1], **Justin DeLos Santos**[1], **Kayvan R. Keshari**[2], **David M. Wilson**[1], **Donna Peehl**[3], **John Kurhanewicz**[1], and **Zhen J. Wang**[1]

[1]Radiology and Biomedical Imaging, University of California San Francisco, San Francisco, CA, United States

[2]Radiology and Molecular Pharmacology Program, Memorial Sloan Kettering Cancer Center, New York, NY, United States

[3]Department of Urology, Stanford University, Stanford, CA, United States

Abstract

Localized renal tumors are increasingly detected incidentally at imaging. Conventional imaging cannot reliably differentiate the 20% of these tumors that are benign from malignant renal cell carcinomas (RCCs), leading to unnecessary surgical resection and resulting morbidity associated with surgery. Here, we investigated hyperpolarized ^{13}C pyruvate metabolism in live patient-derived renal tumor tissue slices using a novel magnetic resonance (MR) -compatible bioreactor platform. We demonstrated for the first time that clear cell RCCs (ccRCCs), which account for 70–80% of all RCCs, have increased lactate production as well as rapid lactate efflux compared to benign renal tumors. This difference is attributed to increased lactate dehydrogenase A and monocarboxylate transporter 4 expression in ccRCCs. This distinctive metabolic phenotype can be used to differentiate RCCs from benign renal tumors using clinically translatable hyperpolarized ^{13}C pyruvate MR.

Keywords

Hyperpolarized ^{13}C magnetic resonance (HP ^{13}C MR); dynamic nuclear polarization (DNP); aerobic glycolysis; lactate efflux; renal cell carcinoma (RCC); patient-derived tissue slice cultures

Introduction

The widespread use of cross-sectional imaging has led to a significant increase in the incidental detection of renal tumors [1], many of which are localized, clinical stage 1 tumors. These tumors exhibit a wide spectrum of benign and malignant histopathology as well as aggressiveness, posing significant challenges for clinical management. Approximately 20% of the clinical stage 1 renal tumors are benign tumors such as

*Correspondence and Reprint Request: Zhen Jane Wang, MD, Department of Radiology and Biomedical Imaging, University of California, San Francisco, San Francisco, CA 94143, Tel: (415) 476-3767, Fax: (415) 514-0414, ; Email: jane.wang@ucsf.edu.

oncocytomas or minimal fat angiomyolipomas [2–5]. These benign tumors cannot be reliably differentiated from renal cell carcinoma (RCC) preoperatively using conventional imaging [6]. Percutaneous tumor biopsy also has its limitations, including low negative predictive value of biopsy for small renal masses, and overlapping histologic features between some benign renal tumors and RCCs [7]. Because of these limitations, localized renal tumors are most frequently treated with surgical resection. This has led to greater than 10,000 unnecessary operations of benign tumors each year in the U.S. alone [8], with inherent risks of surgery, loss of renal function, and cost. Therefore, new non-invasive imaging methods are needed to distinguish benign renal tumors from RCCs in order to guide management.

Increasing evidence has shown that RCCs are strongly linked to abnormal metabolism [9–11]. In particular, increased glycolysis with lactate production (Warburg effect) is a dominant metabolic feature of RCCs. For example, clear cell RCCs, which accounts for 70–80% of all RCCs, have characteristic reprogramming of glucose and energy metabolism that promotes glycolysis and lactate production [12,13]. High expression of monocarboxylate transporters 1 and 4, which are essential for maintaining high level of glycolysis and lactate transport, are associated with more aggressive RCCs [14–16]. These studies provide the rationale for metabolic imaging as a means to differentiate benign renal tumors from RCCs.

Hyperpolarized (HP) ^{13}C magnetic resonance (MR) is a powerful molecular imaging technique that allows rapid and non-invasive investigation of dynamic metabolic and physiological processes that were previously inaccessible by imaging [17]. HP ^{13}C pyruvate is the most widely studied probe to date [18,19], reflecting its central role in cellular metabolism. In particular, pyruvate is reduced to lactate in a reaction catalyzed by the enzyme lactate dehydrogenase (LDH). Several previous studies have shown that *in vivo* HP ^{13}C pyruvate to lactate flux correlates to tumor grade in preclinical cancer models [20,21].

In this study, we compared the HP ^{13}C lactate levels after injection of HP ^{13}C pyruvate in live patient-derived renal tissue slices maintained in a MR-compatible bioreactor. The bioreactor provides a novel platform for the assessment of tissue metabolism in a controlled and physiologic setting [22,23]. We show that clear cell RCCs (ccRCCs) have high lactate production and importantly, they have increased lactate export when compared to benign renal tumors. This suggests that such metabolic phenotype can be explored to non-invasively differentiate ccRCCs from benign renal tumors using clinically translatable hyperpolarized ^{13}C pyruvate MR.

Material and Methods

Patient-derived renal tissue slices

Fresh tissues were obtained from patients undergoing nephrectomy for renal tumors between September 2012 and August 2014 under an institutional review board-approved protocol. Tissue cores (8-mm diameter) of both tumors and adjacent uninvolved normal renal parenchyma were obtained from the nephrectomy specimen [24]. Tissues were precision-cut into 300 to 350 μm thick slices using a Krumdieck slicer (Alabama Research and

Development, Mundford, AL, USA), and then cultured in an incubator at 37°C and 5% CO_2 for 12–18 hours in specialized medium in an angled rotating plate (30 degree) as previously described [25]. Subsequently, 4–6 tissue slices were loaded into a 5-mm MR-compatible bioreactor as previously described [22,23] for the hyperpolarized experiments below. Patient-derived renal slices were obtained from 10 clear cell RCCs (Furhman grade 1: n=1; Furhman grade 2: n=8; Furhman grade 3: n=1), 3 benign renal tumors (oncocytomas: n=2; angiomyolipomas: n=1), and 12 normal renal parenchyma tissues not involved with tumors. These fresh tissue slices were studied in a 3D tissue bioreactor.

MR-compatible 3-dimensional (3D) tissue culture bioreactor experiments

The tissue slices were maintained at physiological conditions in the bioreactor in circulating media at 37°C with 95% air/5% CO_2 via a gas exchanger. All bioreactor experiments were conducted using a 500 MHz Varian Inova (Agilent Technologies, Palo Alto, CA, USA) with a 5-mm, triple-tune, direct-detect, broadband probe. For the HP ^{13}C pyruvate studies, 7.5 μL of 14.2 M [1-^{13}C]pyruvate mixed with 15 mM of the trytl radical (GE Health, Menlo Park, CA, USA) and 2.5 mM gadolinium chelate were polarized on a Hypersense polarizer (Oxford Instruments, Oxford, UK). This was followed by dissolution in 5 mL of 50 mM phosphate buffer. Seven hundred and fifty μL of the resulting 16 mM HP ^{13}C pyruvate solution was injected over 90 seconds into the bioreactor containing the tissue slices. Hyperpolarized ^{13}C MR data were acquired dynamically with a 30 degree flip angle, pulse repetition time of 3 seconds, and for a duration of 300 seconds. ^{31}P spectra were acquired before and after each hyperpolarized ^{13}C study to assess tissue viability using a repetition time of 2 seconds, 2048 averages, and a 90 degree flip angle. The βNTP peak was quantified using the ERETIC method as described previously (26).

Immunohistochemical staining and pathological grading

At the end of the MR experiments, some of the renal tissue slices were rapidly frozen in cryo-embedding medium (Optimal Cutting Temperature Compound) for subsequent histological and immunohistochemical analyses. A clinical pathologist determined the renal tumor histology and grade (Furhman nuclear grading if RCCs) based on hemotoxylin and eosin (H&E) staining. Additionally, the slices were stained for monocarboxylate 4 (MCT4) expression.

Tissue slice mRNA expression and enzyme activity assay

Remaining tissue slices at the end of the bioreactor experiment were immediately frozen and used to measure enzymatic activity and mRNA expression as described previously [22,26]. mRNA expression of LDHA, monocarboxylate 1 (MCT1) and MCT4 was quantified using qRT-PCR. In brief, total RNA was extracted from the tissue slices using an RNAeasy kit (Qiagen, Germantown, MD, USA). Reverse transcription was performed using an iScript cDNA Synthesis kit (BioRad Laboratories, Hercules, CA, USA), and subsequently the cDNA generated was utilized for PCR in triplicate with TaqMan chemistry on the ABI 7900HT (Applied Biosystems, Foster City, CA, USA). Primers for the genes were obtained from Applied Biosystems (Foster City, CA, USA). The gene expression was calculated relative to the housekeeping gene beta-Actin.

LDH activity of tissue slices was measured spectrophotometrically by quantifying the linear decrease in NADH absorbance at varying pyruvate concentrations at 339 nm using a micro-plate reader (Tecan Group Ltd., Mannedorf, Switzerland) [22,26]. The maximum velocity (V_{max}) and the Michaelis–Menten constant (K_m) were estimated using the Lineweaver–Burke plot, and were normalized to the protein content.

Lactate efflux measurement of renal tissue slices

Tissue slices immediately adjacent to those used in the bioreactor experiments were incubated in 2-dimensional (2D) culture in media containing 25 mM [3-^{13}C]pyruvate. The rate of lactate efflux from the tissue slices was evaluated by sampling the medium every 60–120 minutes over 8 hours. The lactate in the medium was measured by ^{1}H MR spectroscopy in an 800 MHz Bruker DRX spectrometer (Billerica, MA, USA) equipped with a cryo-cooled 5-mm triple-axis heteronuclear probe. The J-coupled ^{13}C satellite resonance was quantified using ACD/Labs software as described below.

Data analysis

The MR data was processed and analyzed using ACD/Labs software (Toronto, Canada). The ^{13}C data were processed with minimal line broadening and the dynamic data were summed and expressed as a ratio of the hyperpolarized ^{13}C lactate peak area to that of ^{13}C pyruvate in order to normalize any differences in polarization across experiments. All data are represented as mean ± standard deviation. Two-tailed Student's t-test was used to assess the difference between groups.

Results

Bioenergetics and viability of renal tissue slices in the MR-compatible 3D tissue culture bioreactor

In a prior study, we demonstrated that the MR-compatible 3D bioreactor maintains tissue viability and provides reproducible HP ^{13}C MR data [22]. In this study, it allowed the metabolic evaluation of 60–90 mg of living tissue and had excellent B_0 field homogeneity (average water line width at half maximum was 12.2 ± 0.68 Hz). ^{31}P MR spectroscopy was employed to monitor changes in renal tissue slice bioenergetics during the bioreactor studies. Figure 1A shows a representative ^{31}P spectrum of ccRCC tissue slices. NMR signals for the nucleoside triphosphates (NTPs: γNTP, αNTP, and βNTP), nicotinamide adenine dinucleotide/uridine diphosphates (NAD/UDP), phosphocholine (PC), inorganic phosphate (P_i), and glycerol phosphocholine (GPC) were readily visible. The βNTP content was unchanged following the injection of HP ^{13}C pyruvate, indicating maintenance of tissue bioenergetics during the course of hyperpolarized experiments.

Figure 1B shows the varying levels of phospholipids in the renal tissue slices. Interestingly, the PC level in the benign renal tumors was significantly higher than levels in either the normal renal parenchyma (p=0.019) or ccRCC (p=0.008) tissues. This finding is similar to that from a prior ^{1}H high-resolution study of renal tissue extracts [27]. It suggests that, while PC has been used as a biomarker of proliferation and aggressiveness in other types of cancer [28], it has limited value in stratifying renal tumor aggressiveness. PC is converted from

choline by the enzyme choline kinase-alpha (CHKA) in the phosphatidylcholine synthesis (Kennedy) pathway. A prior study reported that functional interaction between CHKA, epidermal growth factor receptor (EGFR) and c-Src is required for cell proliferation [29]. Such functional interactions may explain the lack of direct correlation between the PC level and renal tumor aggressiveness in our study. GPC, on the other hand, was significantly higher in both benign renal tumors and ccRCCs compared to normal renal parenchyma tissue (p=0.027 and 0.003, respectively). While GPC is an osmolyte in the renal medulla, it is also involved in cell membrane recycling [30]. The biological basis of elevated GPC levels in the renal tumor tissues requires further investigation.

Hyperpolarized ^{13}C pyruvate metabolism of renal tissue slices in the 3D MR-compatible bioreactor

Figure 2A illustrates the scheme of ^{13}C-labeled carbon flux used to detect [1-^{13}C]pyruvate metabolism during the HP MR experiment. After injection of hyperpolarized [1-^{13}C]pyruvate into the bioreactor, the ^{13}C lactate level in the renal tissue slices was assessed in real time. The ^{13}C lactate spectrum had excellent signal to noise ratio (SNR) of 15 ± 2 (Figure 2B). The benign renal tumors and ccRCCs showed 2.7-fold and 1.7-fold higher hyperpolarized ^{13}C lactate levels (Figure 2C), consistent with increased aerobic glycolysis, when compared to normal renal parenchymal tissues (p=0.023 and 0.017, respectively). However, the observed ^{13}C lactate level was 59% lower in ccRCCs than in benign renal tumors. Prior studies of human RCC cells in a similar continuous perfusion system showed that rapidly exported ^{13}C lactate quickly flows out of the MR-sensitive volume without contributing to the measured hyperpolarized ^{13}C lactate signal [26]. Therefore, we hypothesized that the apparent lower ^{13}C lactate level in ccRCC compared to benign renal tumors may be a result of rapid lactate efflux in ccRCCs, and tested this hypothesis in the lactate efflux measurements described below.

HP ^{13}C alanine was consistently detected in the normal renal tissues with a SNR of at least 3. Alanine was not detectable in the benign renal tumor tissues, and it was occasionally observed (in ~30% of the cases) at low levels in the ccRCC tissues. The low alanine level observed in the RCC tissues is consistent with a prior study by our group that demonstrated lower alanine levels in immortalized human RCC cells compared to normal renal tubular cells [26].

Tissue analysis confirms that ccRCCs have higher lactate production and efflux than benign renal tumors

To test the hypothesis that ccRCCs have higher lactate production and efflux than benign renal tumors, we assayed mRNA expression and enzymatic activity of LDH, and mRNA expression of MCT1 and MCT4, in the tissue slices. The LDHA gene encodes the M subunits of LDH, which catalyzes the conversion between pyruvate and lactate. MCT1 mediates pyruvate transport into cells, and MCT4 mediates efflux of lactate out of cells [31,32]. Mean LDHA mRNA expression was significantly higher in ccRCCs (171 ± 106) compared to either normal renal tissues (41 ± 25) or benign tumors (50 ± 36) (p=0.001 and 0.016, respectively) (Figure 3A). Correspondingly LDH activity was significantly higher in ccRCC compared to normal renal tissues (p=0.020) and benign tumors (p=0.030), by 2.4-

and 1.7-fold, respectively (Figure 3A). Similarly, mRNA expression of MCT1 (figure 3B) was significantly higher in ccRCCs compared to normal renal tissues (3-fold higher, p=0.006) and benign tumors (8-fold higher, p=0.002). The higher expression of LDHA and MCT1 in ccRCCs compared to benign renal tumors is consistent with a higher level of glycolysis and lactate production in ccRCCs.

MCT4 mRNA expression in the ccRCCs was significantly higher than in normal renal tissues (4-fold higher, p=0.021) and benign tumors (11-fold higher, p=0.045) (Figure 4B). Corresponding immunohistochemical staining also showed progressively increased MCT4 staining from normal renal tissues to ccRCCs (Figure 4A). These data suggest that ccRCCs have a high rate of lactate efflux. To further verify that the higher MCT4 expression in ccRCCs resulted in increased lactate efflux, we quantified the rate of lactate efflux in the tissue slices in a 2D culture by labeling with [3-^{13}C]pyruvate (Figure 4C). The incubating medium was sampled intermittently for up to 8 hours and the [3-^{13}C]lactate was measured using high-resolution NMR spectroscopy. The normal renal tissues and benign tumors had similar lactate efflux rates of 1.83 ± 1.98 nmols/min and 2.32 ± 0.89 nmols/min, respectively, while ccRCCs had a significantly higher efflux rate of 5.04 ± 1.82 nmols/min (p=0.013 and 0.002, respectively). Taken together, these observations support the hypothesis that ccRCCs have the highest lactate production and efflux compared to benign renal tumors and normal renal tissues. The rapid lactate efflux out of the cells is the dominant factor resulting in the observed apparent lower HP ^{13}C lactate level in ccRCCs than benign renal tumors.

Discussion and Conclusion

An unmet need in the management of patients with localized renal tumors is the lack of imaging biomarkers that can reliably discriminate benign tumors from RCCs. In this study, we investigated pyruvate metabolism in live patient-derived renal tumor tissues using hyperpolarized [1-^{13}C]pyruvate, a HP ^{13}C MR probe that has been used in patient studies [33]. We showed that high lactate production and rapid lactate efflux are characteristic features of clear cell RCC, which comprise the majority of RCCs, and that this metabolic feature may be used to differentiate cancers from benign renal tumors.

Increasing evidence has shown that RCCs are strongly linked to abnormal metabolism [9,10,34]. In particular, increased glycolysis with lactate production is a dominant metabolic feature of many RCCs. Lactate is exported out of the cells, predominantly mediated by MCT4, a proton-coupled lactate transporter. Rapid lactate export plays a key role in maintaining high levels of lactate production, acidifying the tumor interstitium and promoting invasion and metastasis, all key features of cancers [35,36]. The potential importance of MCT4 in RCCs was suggested by a recent study which showed that MCT4 protein expression in clear cell RCCs was associated with poorer relapse-free survival, and correlated with Fuhrman nuclear grade [15]. In our current work, we showed that live patient–derived clear cell RCC tissues have more rapid lactate efflux, as a result of high MCT4 expression, compared to benign renal tumors. Such differential expression and the resultant lactate efflux rate may be explored noninvasively using HP ^{13}C MR. In our current pre-clinical study which utilized an *ex vivo* system, the higher lactate export in RCCs

compared to benign tumors was inferred from a combination of HP ^{13}C MR and steady-state labeling experiments. However, it is possible to discriminate the local environment of HP metabolites using diffusion-weighted HP ^{13}C MR *in vivo* [37]. Our findings provide rationale for such *in vivo* studies, and work is ongoing to utilize *in vivo* diffusion-weighted HP ^{13}C MR to directly interrogate the relative amount of intracellular versus extracellular lactate. Additionally, *in vivo* HP imaging will also permit the assessment of total lactate as a marker of lactate production in renal tumors. During the time frame of the HP studies, the lactate exported out of the renal tumor cells is likely to remain within the tumor interstitium, and the combined intra- and extracellular lactate can be measured. The lactate production, in addition to the rate of lactate efflux, can provide complementary biomarkers of renal tumor aggressiveness.

The development of novel imaging markers of RCC presence and aggressiveness has been impeded by the lack of robust models that recapitulate human disease. Available preclinical models are predominantly based on immortalized aggressive RCC cells either grown in culture or implanted in animals. We previously studied pyruvate metabolism in immortalized RCC cells [26], but were not able to investigate the metabolism of benign renal tumors as there are no existing preclinical models of benign human renal tumors. Immortalized RCC cells also have unusually high proliferation indices compared to patient-derived renal tumor tissues, which may be reflected in the observed metabolism. Furthermore, immortalized cell models do not capture the complex tumor cell-matrix interactions which occur in human renal tumors, and which are likely important for tumor metabolism. To overcome these difficulties, we utilized in this study a patient-derived renal tumor slice model for the metabolic assessment of intact living human tissues. The novel MR-compatible micro-engineered bioreactor permits evaluation of living tissue metabolism in a physiological environment, and has been previously validated by our group in prostate cancer studies [22]. The combination of primary human renal tumor tissue slices and MR-compatible bioreactor provides a unique and realistic model for HP ^{13}C biomarker discovery in renal tumors prior to patient studies.

The main limitation of our study is the small number of benign renal tumors. Benign tumors tend to be smaller in size, and limited tissues were available for this research study without potentially compromising the tissues required for clinical diagnosis. Nonetheless, we have shown a significant difference in both the hyperpolarized ^{13}C data and the tissue correlative findings between benign tumors and RCCs. The results of the study provide motivation for future clinical studies of HP ^{13}C pyruvate MR in patients with renal tumors. Another limitation of our study is that we have only included clear cell RCCs, and not other subtypes of RCCs. This in part reflects the fact that ccRCCs comprise the majority of RCCs (70–80%), and we did not obtain sufficient numbers of other subtypes of RCCs to include in our analysis. Along the same line, the majority of the ccRCC tissues obtained were grade 1 or 2. Accordingly, there was an insufficient number of higher grade (grade 3 or 4) ccRCCs to perform separate analysis based on grade. Future studies are warranted to assess any potential grade-dependent findings. Development of imaging markers that can reliably differentiate low from high grade RCCs is of great clinical interest given the increasing recognition that low grade indolent RCCs may be treated conservatively via active surveillance rather than surgical resection [38]. Another limitation is that the renal tumor

tissue slices used in the 2D culture experiments were not the same ones used in the 3D bioreactor experiments. Although renal tumors do have intra-tumoral heterogeneity, the tumor tissue slices were from the same core, and were immediately adjacent to each other. Therefore, we believe any potential heterogeneity is not likely to affect the overall results.

Notwithstanding these limitations, we showed that high lactate production and rapid lactate efflux are dominant features of ccRCCs. These features can be explored to noninvasively differentiate cancers from benign renal tumors using hyperpolarized ^{13}C pyruvate MR, especially when combined with diffusion weighting. These initial findings provide strong motivation for developing hyperpolarized ^{13}C MR for clinical evaluation of renal tumors. Notably, the safety and feasibility of HP ^{13}C pyruvate has already been demonstrated in the phase I clinical trial in prostate cancer patients [33], which opens doors for potential clinical translation of this technology to other diseases. Additionally, work is ongoing to develop multi-channel ^{13}C MR coil to provide optimal signal reception in abdominal organs for clinical studies. These technical advances will facilitate the translation of this emerging molecular imaging tool for assessment of renal tumors, a disease of increasing frequency, with the ultimate goal of guiding treatment selection.

Acknowledgments

We thank Rosalie Nolley, Romelyn Delos Santos, Laura Tabatabai, Ailin Hansen, Dave Korenchen, Sukumar Subramaniam, Bertram Koelsch and Jessie Lee for assistance in performing experiments.

qRT-PCR analysis was conducted at the Genome Analysis Core Facility, Helen Diller Family Comprehensive Cancer Center, University of California, San Francisco

Grant Sponsor: National Institutes of Health (R01 EB013427, R01 EB017449, R01 CA183071, P41 EB013598, R21 EB005363, R00 EB014328, P30 CA008748, R01 CA166655, and R01 DK097357) and Department of Defense (USAMRMC CA110032)

Abbreviations used

2D	2-dimensional
3D	3-dimensional
HP	hyperpolarized
LDH	lactate dehydrogenase
MCT1	monocarboxylate 1
MCT4	monocarboxylate 4
MR	magnetic resonance
MRS	magnetic resonance spectroscopy
DNP	dynamic nuclear polarization
RCC	renal cell carcinoma
ccRCC	clear cell renal cell carcinoma
NTP	nucleoside triose phosphate

MCT	monocarboxylate transporter
LDH	lactate dehydrogenase
TCA	tricarboxylic acid
H & E	hemotoxylin and eosin
mRNA	messenger ribonucleic acid
cDNA	complimentary deoxyribonucleic acid
qRT-PCR	quantitative reverse transcription polymerase chain reaction
NADH	nicotinamide adenine dinucleotide
PC	phosphocholine
Pi	inorganic phosphate
GPC	glycerol phosphocholine
CHKA	choline kinase-alphs
EGFR	epidermal growth factor receptor
SNR	signal to noise ratio

References

1. Sun M, Thuret R, Abdollah F, Lughezzani G, Schmitges J, Tian Z, Shariat SF, Montorsi F, Patard JJ, Perrotte P, Karakiewicz PI. Age-adjusted incidence, mortality, and survival rates of stage-specific renal cell carcinoma in North America: a trend analysis. European Urology. 2010 ed. 2011 Jan; 59(1):135–141.
2. Frank I, Blute ML, Cheville JC, Lohse CM, Weaver AL, Zincke H. Solid renal tumors: an analysis of pathological features related to tumor size. J Urol. 2003 Dec; 170(6 Pt 1):2217–2220. [PubMed: 14634382]
3. DeRoche T, Walker E, Magi-Galluzzi C, Zhou M. Pathologic characteristics of solitary small renal masses: can they be predicted by preoperative clinical parameters? Am J Clin Pathol. 2008 Oct; 130(4):560–564. [PubMed: 18794048]
4. Snyder ME, Bach A, Kattan MW, Raj GV, Reuter VE, Russo P. Incidence of benign lesions for clinically localized renal masses smaller than 7 cm in radiological diameter: influence of sex. J Urol. 2006 Dec; 176(6 Pt 1):2391–2395. discussion2395–6. [PubMed: 17085108]
5. Murphy AM, Buck AM, Benson MC, McKiernan JM. Increasing detection rate of benign renal tumors: evaluation of factors predicting for benign tumor histologic features during past two decades. Urology. 2009 ed. 2009 Jun; 73(6):1293–1297.
6. Woo S, Cho JY. Imaging Findings of Common Benign Renal Tumors in the Era of Small Renal Masses: Differential Diagnosis from Small Renal Cell Carcinoma: Current Status and Future Perspectives. Korean J Radiol. 2015; 16(1):99. [PubMed: 25598678]
7. Ljungberg B, Hanbury DC, Kuczyk MA, Merseburger AS, Mulders P, Patard JJ, Sinescu IC. Guidelines on renal cell carcinoma. European Association of Urology. 2008; 1:1–22.
8. Asnis-Alibozek AG, Fine MJ, Russo P, McLaughlin T, Farrelly EM, LaFrance N, Lowrance W. Cost of care for malignant and benign renal masses. Am J Manag Care. 2013 Aug; 19(8):617–624. [PubMed: 24304211]
9. Pinthus, JH.; Whelan, KF.; Gallino, D.; Lu, J-P.; Rothschild, N. Canadian Urological Association Journal. Vol. 5. Canadian Medical Association; 2011 Aug 1. Metabolic features of clear-cell renal cell carcinoma: mechanisms and clinical implications; p. 274-282.

10. Zaravinos A, Pieri M, Mourmouras N, Anastasiadou N, Zouvani I, Delakas D, Deltas C. Altered metabolic pathways in clear cell renal cell carcinoma: A meta-analysis and validation study focused on the deregulated genes and their associated networks. Oncoscience. 2014; 1(2):117–131. [PubMed: 25594006]
11. Hakimi AA, Reznik E, Lee C-H, Creighton CJ, Brannon AR, Luna A, Aksoy BA, Liu EM, Shen R, Lee W, Chen Y, Stirdivant SM, Russo P, Chen Y-B, Tickoo SK, Reuter VE, Cheng EH, Sander C, Hsieh JJ. An Integrated Metabolic Atlas of Clear Cell Renal Cell Carcinoma. Cancer Cell. 2016 Jan 11; 29(1):104–116. [PubMed: 26766592]
12. Unwin RD, Craven RA, Harnden P, Hanrahan S, Totty N, Knowles M, Eardley I, Selby PJ, Banks RE. Proteomic changes in renal cancer and co-ordinate demonstration of both the glycolytic and mitochondrial aspects of the Warburg effect. Proteomics. 2003 Aug; 3(8):1620–1632. [PubMed: 12923786]
13. Singer S, Souza K, Thilly WG. Pyruvate utilization, phosphocholine and adenosine triphosphate (ATP) are markers of human breast tumor progression: a 31P- and 13C-nuclear magnetic resonance (NMR) spectroscopy study. Cancer Research. 1995 Nov 15; 55(22):5140–5145. [PubMed: 7585561]
14. Fisel P, Kruck S, Winter S, Bedke J, Hennenlotter J, Nies AT, Scharpf M, Fend F, Stenzl A, Schwab M, Schaeffeler E. DNA Methylation of the SLC16A3 Promoter Regulates Expression of the Human Lactate Transporter MCT4 in Renal Cancer with Consequences for Clinical Outcome. Clinical Cancer Research. 2013 Sep 16; 19(18):5170–5181. [PubMed: 23881922]
15. Fisel P, Stühler V, Bedke J, Winter S, Rausch S, Hennenlotter J, Nies AT, Stenzl A, Scharpf M, Fend F, Kruck S, Schwab M, Schaeffeler E. MCT4 surpasses the prognostic relevance of the ancillary protein CD147 in clear cell renal cell carcinoma. Oncotarget. 2015 Oct 13; 6(31):30615–30627. [PubMed: 26384346]
16. Gerlinger, M.; Santos, CR.; Spencer-Dene, B.; Martinez, P.; Endesfelder, D.; Burrell, RA.; Vetter, M.; Jiang, M.; Saunders, RE.; Kelly, G.; Dykema, K.; Rioux-Leclercq, N.; Stamp, G.; Patard, J-J.; Larkin, J.; Howell, M.; Swanton, C. J Pathol. Vol. 227. Blackwell Publishing; 2012 Apr 18. Genome-wide RNA interference analysis of renal carcinoma survival regulators identifies MCT4 as a Warburg effect metabolic target; p. 146-156.
17. Keshari, KR.; Wilson, DM. Chem Soc Rev. Vol. 43. The Royal Society of Chemistry; 2014. Chemistry and biochemistry of 13C hyperpolarized magnetic resonance using dynamic nuclear polarization; p. 1627-1659.
18. Sriram, R.; Kurhanewicz, J.; Vigneron, DB. eMagRes. Vol. 3. Chichester, UK: John Wiley & Sons, Ltd; 2014 Dec 15. Hyperpolarized Carbon-13 MRI and MRS Studies; p. 311-324.
19. Chaumeil MM, Najac C, Ronen SM. Studies of Metabolism Using (13)C MRS of Hyperpolarized Probes. Meth Enzymol. 2015; 561:1–71. [PubMed: 26358901]
20. Albers MJ, Bok R, Chen AP, Cunningham CH, Zierhut ML, Zhang VY, Kohler SJ, Tropp J, Hurd RE, Yen Y-F, Nelson SJ, Vigneron DB, Kurhanewicz J. Hyperpolarized 13C lactate, pyruvate, and alanine: noninvasive biomarkers for prostate cancer detection and grading. Cancer Research. 2008 Oct 15; 68(20):8607–8615. [PubMed: 18922937]
21. Kurhanewicz J, Vigneron DB, Brindle K, Chekmenev EY, Comment A, Cunningham CH, DeBerardinis RJ, Green GG, Leach MO, Rajan SS, Rizi RR, Ross BD, Warren WS, Malloy CR. Analysis of cancer metabolism by imaging hyperpolarized nuclei: prospects for translation to clinical research. Neoplasia. 2011 Feb; 13(2):81–97. [PubMed: 21403835]
22. Keshari KR, Sriram R, Van Criekinge M, Wilson DM, Wang ZJ, Vigneron DB, Peehl DM, Kurhanewicz J. Metabolic reprogramming and validation of hyperpolarized 13C lactate as a prostate cancer biomarker using a human prostate tissue slice culture bioreactor. Prostate. 2013 Aug; 73(11):1171–1181. [PubMed: 23532911]
23. Keshari KR, Wilson DM, Van Criekinge M, Sriram R, Koelsch BL, Wang ZJ, VanBrocklin HF, Peehl DM, O'Brien T, Sampath D, Carano RAD, Kurhanewicz J. Metabolic response of prostate cancer to nicotinamide phophoribosyltransferase inhibition in a hyperpolarized MR/PET compatible bioreactor. Prostate. 2015 Oct; 75(14):1601–1609. [PubMed: 26177608]
24. Thong AE, Zhao H, Ingels A, Valta MP, Nolley R, Santos J, Young SR, Peehl DM. Tissue slice grafts of human renal cell carcinoma: an authentic preclinical model with high engraftment rate and metastatic potential. Urol Oncol. 2014 Jan; 32(1):43.e23–43.e30. [PubMed: 23911681]

25. Maund, SL.; Nolley, R.; Peehl, DM. Lab Invest. Vol. 94. Nature Publishing Group; 2013 Dec 2. Optimization and comprehensive characterization of a faithful tissue culture model of the benign and malignant human prostate; p. 208-221.
26. Keshari KR, Sriram R, Koelsch BL, Van Criekinge M, Wilson DM, Kurhanewicz J, Wang ZJ. Hyperpolarized 13C-pyruvate magnetic resonance reveals rapid lactate export in metastatic renal cell carcinomas. Cancer Research. 2013 Jan 15; 73(2):529–538. [PubMed: 23204238]
27. Tugnoli V, Poerio A, Tosi MR. Phosphatidylcholine and cholesteryl esters identify the infiltrating behaviour of a clear cell renal carcinoma: 1H, 13C and 31P MRS evidence. Oncol Rep. 2004 Aug 1; 12(2):353–356. [PubMed: 15254701]
28. Podo F. Tumour phospholipid metabolism. NMR Biomed. 1999 Nov; 12(7):413–439. [PubMed: 10654290]
29. Miyake, T.; Parsons, SJ. Oncogene. Vol. 31. NIH Public Access; 2011 Aug 8. Functional interactions between Choline kinase α, epidermal growth factor receptor and c-Src in breast cancer cell proliferation; p. 1431-1441.
30. Glunde, K.; Bhujwalla, ZM.; Ronen, SM. Nat Rev Cancer. Vol. 11. Nature Publishing Group; 2011 Dec 1. Choline metabolism in malignant transformation; p. 835-848.
31. Dimmer KS, Friedrich B, Lang F, Deitmer JW, Bröer S. The low-affinity monocarboxylate transporter MCT4 is adapted to the export of lactate in highly glycolytic cells. Biochem J. 2000 Aug 15; 350(Pt 1):219–227. [PubMed: 10926847]
32. Harris T, Eliyahu G, Frydman L, Degani H. Kinetics of hyperpolarized 13C1-pyruvate transport and metabolism in living human breast cancer cells. Proc Natl Acad Sci USA. 2009 Oct 27; 106(43):18131–18136. [PubMed: 19826085]
33. Nelson SJ, Kurhanewicz J, Vigneron DB, Larson PEZ, Harzstark AL, Ferrone M, Van Criekinge M, Chang JW, Bok R, Park I, Reed G, Carvajal L, Small EJ, Munster P, Weinberg VK, Ardenkjaer-Larsen JH, Chen AP, Hurd RE, Odegardstuen L-I, Robb FJ, Tropp J, Murray JA. Metabolic Imaging of Patients with Prostate Cancer Using Hyperpolarized [1-13C]Pyruvate. Sci Transl Med. 2013 Aug 14.5(198):198ra108.
34. Yang, OCY.; Maxwell, PH.; Pollard, PJ. Kidney Int. Vol. 84. Nature Publishing Group; 2013 Oct 1. Renal cell carcinoma: translational aspects of metabolism and therapeutic consequences; p. 667-681.
35. Parks, SK.; Chiche, J.; Pouysségur, J. Nat Rev Cancer. Vol. 13. Nature Publishing Group; 2013 Aug 23. Disrupting proton dynamics and energy metabolism for cancer therapy; p. 611-623.
36. Gatenby RA, Gillies RJ. A microenvironmental model of carcinogenesis. Nat Rev Cancer. 2008 Jan; 8(1):56–61. [PubMed: 18059462]
37. Koelsch BL, Reed GD, Keshari KR, Chaumeil MM, Bok R, Ronen SM, Vigneron DB, Kurhanewicz J, Larson PEZ. Rapid in vivo apparent diffusion coefficient mapping of hyperpolarized (13) C metabolites. Magn Reson Med. 2015 Sep; 74(3):622–633. [PubMed: 25213126]
38. Van Poppel H, Joniau S. Is Surveillance an Option for the Treatment of Small Renal Masses? European Urology. 2007 Nov; 52(5):1323–1330. [PubMed: 17669584]

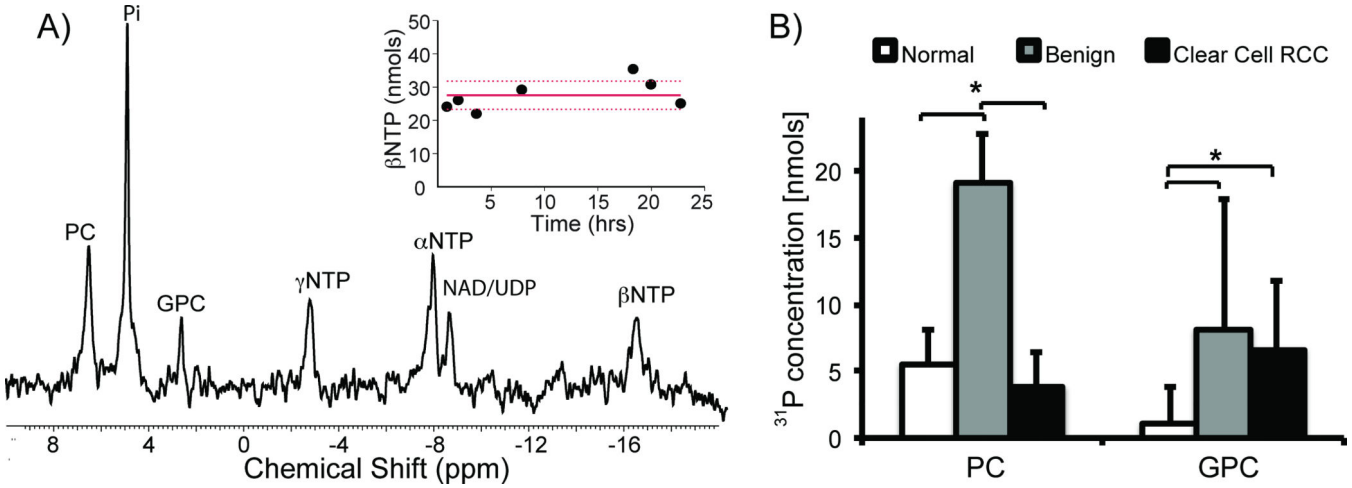

Figure 1.

Bioenergetics of renal tissue slices. A) ^{31}P spectrum of tissue slices (~80mg) from a grade 2 ccRCC. The inset shows the maintenance of tissue viability with unchanged βNTP concentration of tissue slices continuously perfused in the bioreactor for over 24 hours. B) Bar graph of the varying levels of phospholipids in renal tissue slices (n=10 for normal renal parenchymal tissue, n=10 for ccRCCs, and n=3 for benign renal tumors). PC concentration in the benign renal tumors is significantly higher than both the normal renal parenchyma (p=0.019) and ccRCC (p=0.008) tissues. GPC, on the other hand, was significantly higher in both benign renal tumors and ccRCCs compared to normal renal parenchyma tissue (p=0.027 and 0.003, respectively). White bars=normal renal parenchymal tissue, gray bars=benign renal tumors, and black bars=ccRCCs, with standard deviation error bars.

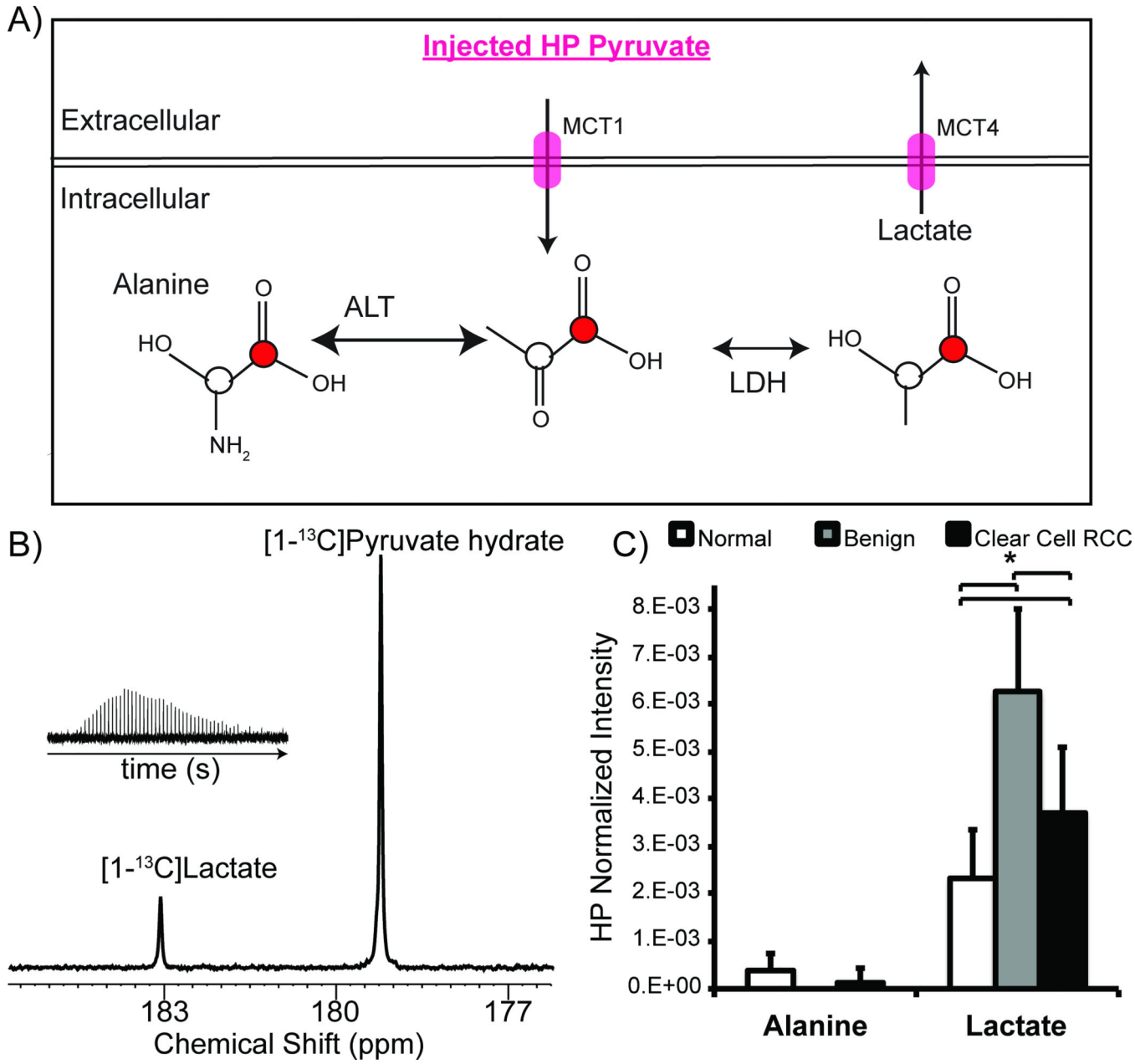

Figure 2.

Hyperpolarized [1-^{13}C]pyruvate metabolism of renal tissue slices. A) Schematic illustrating the metabolism of hyperpolarized [1-^{13}C]pyruvate to [1-^{13}C] lactate and [1-^{13}C] alanine, catalyzed by lactate dehydrogenase (LDH) and alanine aminotransaminase (ALT), respectively. ^{13}C pyruvate is transported intracellularly via monocarboxylate transporter 1 (MCT1), and ^{13}C lactate is exported out of the cells via monocarboxylate transporter 4 (MCT4). B) Representative hyperpolarized ^{13}C spectrum of grade 2 ccRCC tissue slices. Inset shows the lactate kinetics over 5 minutes. C) Bar graphs of normalized hyperpolarized [1-^{13}C] lactate and [1-^{13}C] alanine to the injected pyruvate in the tissue slices. Benign renal tumors and ccRCCs show 2.7 fold and 1.7 fold higher hyperpolarized ^{13}C lactate levels,

consistent with increased aerobic glycolysis, when compared to normal renal parenchymal tissues. The observed ^{13}C lactate level is 59% lower in ccRCCs than benign renal tumors. White bars = normal renal tissue, gray bars = benign renal tumors and black bars=ccRCC, with standard deviation error bars.

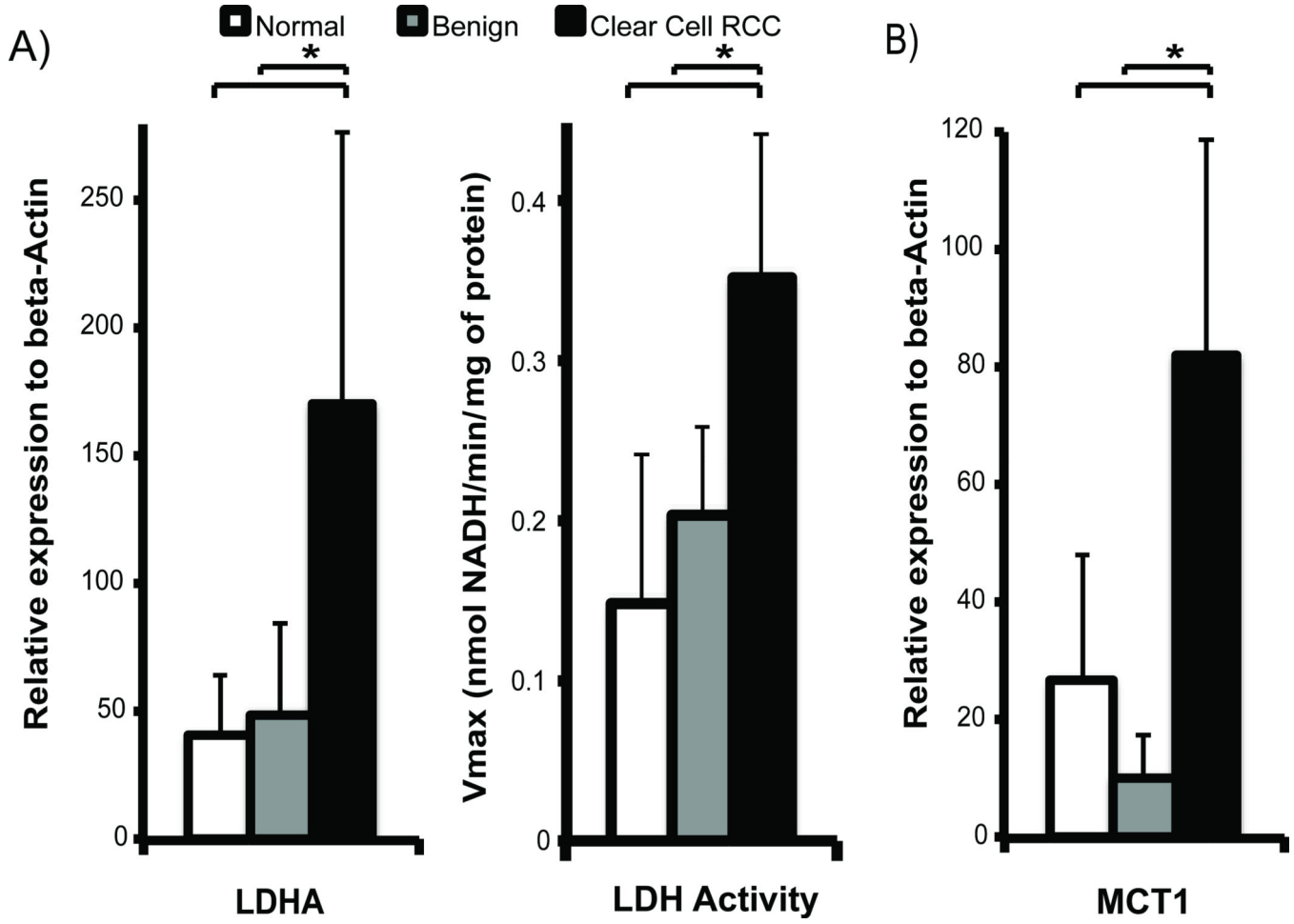

Figure 3.

LDHA expression and LDH activity, and MCT1 expression in renal tissue slices. A) Mean LDHA mRNA expression is higher in ccRCCs compared to either normal renal tissues or benign tumors (p=0.001 and 0.016, respectively), and the LDH activity was also correspondingly higher in ccRCC than normal renal tissues (p=0.020) and benign tumors (p=0.030). B) MCT1 expression is significantly higher in ccRCCs than both normal renal tissues (p=0.006) and benign tumors (p=0.002). The sample size of the tissues used for mRNA analyses is as follows: n=11 for normal renal tissue, n=3 for benign renal tumors, and n=7 for ccRCCs. White bars=normal renal tissue, gray bars=benign renal tumors, and black bars=ccRCC, with standard deviation error bars.

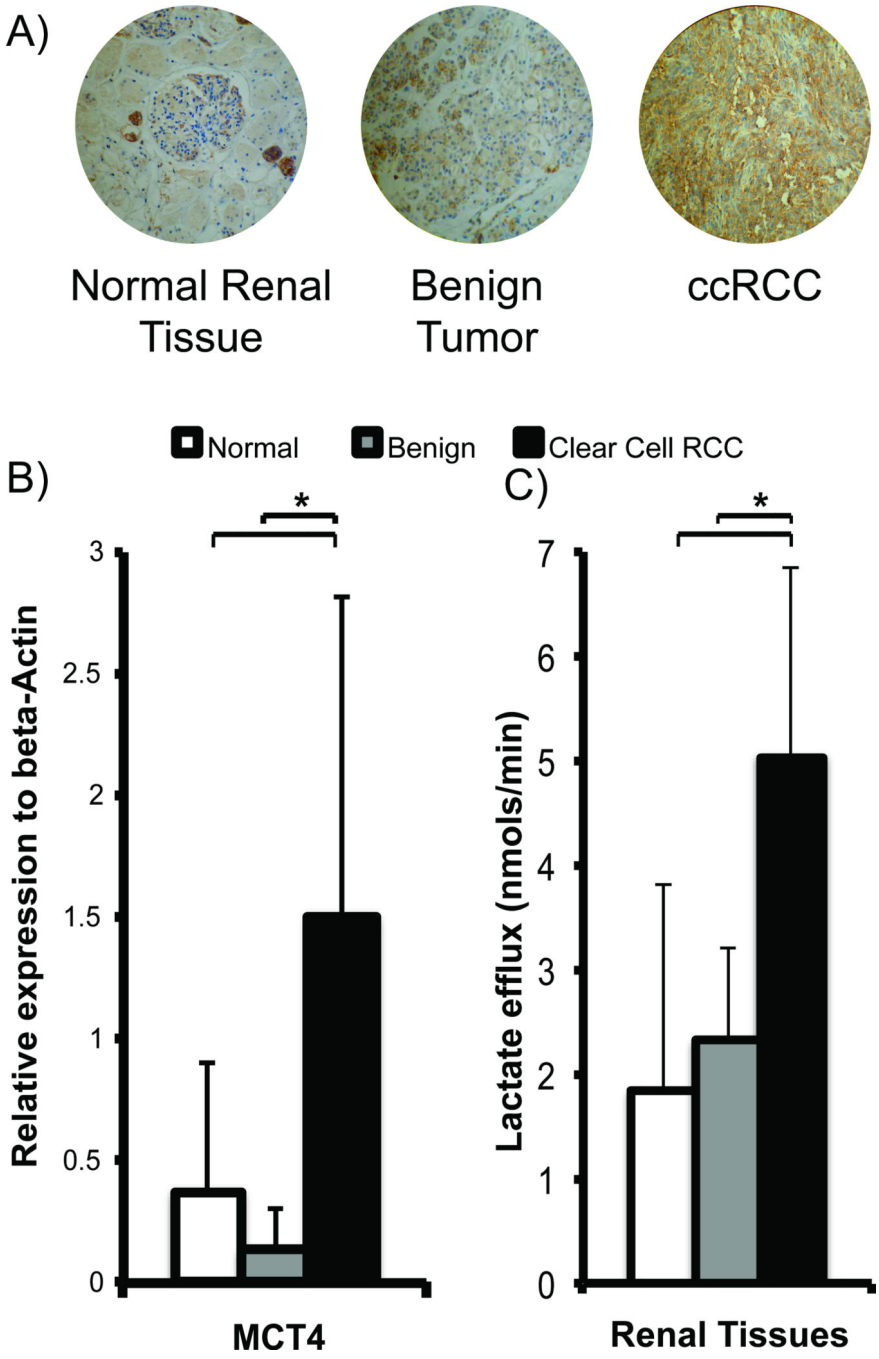

Figure 4.

Renal tissue MCT4 expression and lactate efflux. A) Representative images of MCT4 immunohistochemical staining show increased MCT4 staining (brown staining) in ccRCCs compared to benign renal tumors and normal renal parenchymal tissues. B) ccRCCs show the highest MCT4 mRNA expression compared to normal renal parenchymal tissues (p=0.021), and benign renal tumors (p=0.045). C) ccRCCs show the highest rate of lactate efflux compared to normal renal parenchymal tissues (p=0.013), and benign renal tumors (p=0.002). N=11 for normal renal tissue, n=3 for benign renal tumors, and n=7 for ccRCCs.

White bars = normal renal tissue, gray bars= benign renal tumors and black bars=ccRCC, with standard deviation error bars.